energies

MDPI

Article

Experimental Investigation and Calculation of Convective Heat Transfer in Two-Component Gas–Liquid Flow Through Channels Packed with Metal Foams

Roman Dyga and Małgorzata Płaczek *

Department of Process and Environmental Engineering, Faculty of Mechanical Engineering, Opole University of Technology, Mikolajczyka 5, 45-271 Opole, Poland; r.dyga@po.edu.pl
* Correspondence: m.placzek@po.edu.pl

Abstract: This paper presents a study on heat transfer in two-phase mixtures (air–water and air–oil) flowing through heated horizontal channels filled with open-cell aluminum foams characterized by porosities of 92.9–94.3% and pore densities of 20, 30, and 40 PPI. The research included mass flux densities ranging from 2.82 to 284.7 kg/(m^2·s) and heat flux densities from 5.3 to 35.7 kW/m^2. The analysis examined the effects of flow conditions, fluid properties, and foam geometry on the intensity of heat transfer from the heated walls of the channel to the fluid. Results indicate that the heat transfer coefficient in two-component non-boiling flow exceeds that of single-phase flow, primarily due to fluid properties and velocities, with minimal impact from flow structures or foam geometry. An assessment of existing methods for predicting heat transfer coefficients in gas–liquid and boiling flows revealed significant discrepancies—up to several hundred percent—between measured and predicted values. To address these issues, a novel computational method was developed to accurately predict heat transfer coefficients for two-component non-boiling flow through metal foams.

Keywords: gas–liquid flow; heat transfer; open-cell metal foam; heat transfer coefficient calculation methods

check for updates

Citation: Dyga, R.; Płaczek, M. Experimental Investigation and Calculation of Convective Heat Transfer in Two-Component Gas–Liquid Flow Through Channels Packed with Metal Foams. *Energies* **2024**, *17*, 5250. https://doi.org/10.3390/en17215250

Academic Editor: Efstathios E. Michaelides

Received: 23 September 2024
Revised: 16 October 2024
Accepted: 18 October 2024
Published: 22 October 2024

Copyright: © 2024 by the authors. Licensee MDPI, Basel, Switzerland. This article is an open access article distributed under the terms and conditions of the Creative Commons Attribution (CC BY) license (https://creativecommons.org/licenses/by/4.0/).

1. Introduction

In the past three decades, advancements in processing technology have enabled the development of innovative, lightweight, and durable materials that find wide application in mechanical, structural, electrical, and thermal engineering. Furthermore, progress in the industrial production of multifunctional cellular materials in standard configurations and geometries has opened up new possibilities for their use in various areas of engineering [1–5]. Open-cell metal foams, classified as cellular materials, are eco-friendly and possess features such as low weight, porosity, fire resistance, and non-toxicity. They offer a long service life and represent a robust alternative to conventional materials [6,7]. Open-cell metal foams are particularly notable for their low density (e.g., 0.45 kg/m^3), high surface area density (500–10,000 m^2/m^3), and excellent thermal and electrical conductivity (e.g., ∼200 W/m·K for aluminum and ∼400 W/m·K for copper) [8]. The high surface area of metal foam struts enhances heat transfer through conduction, improves mixing in both single-phase and multiphase systems, and boosts efficiency by increasing the Nusselt number and disrupting the thermal boundary layer [7,9,10]. Their lightweight structure (5–25% metal, 75–95% gas) combines high strength and rigidity with a large surface area, making them ideal for enhancing energy absorption and heat transfer in heat exchangers [11–23], heat sinks and solar collectors [24–33], fuel cells [34–37], and heat pipes [6,10,38].

The literature review reveals that research on thermal phenomena involving open-cell metal foams predominantly focuses on single-phase fluids, such as air or water. In contrast, studies on heat transfer in two-phase flows typically investigate scenarios where a single substance, such as water or a refrigerant, undergoes phase transitions during boiling or

condensation processes. Metal foams in flow boiling processes significantly increase the nucleation rate due to the increased heat exchange area and intensified fluid disturbance, which greatly improves heat transfer efficiency.

Studies have shown that metal foams enhance boiling heat transfer in various configurations, including pipes [39–45], channels [46], heat exchangers and evaporators [47]. Recent experimental and numerical studies on flow boiling in metal foam tubes were conducted by Nosrati et al. [48], Haertlé [49] and Liaw et al. [50].

Zhu et al. [39] experimentally investigated the effect of copper foam (with 0.95 porosity and 5 or 10 PPI) on enhancing heat transfer during convective flow boiling of oil mixtures and refrigerant (R410a) in tubes. They observed a 1.85-fold increase in the heat transfer coefficient with copper foam, although this enhancement was diminished in the presence of oil. They also developed an empirical correlation to capture these effects. In 2014, Zhu et al. [51] extended their research to refrigerant flow in foam-filled tubes of different diameters, finding up to 220% improvement in heat transfer and transitions in flow patterns from stratified to annular flow. They noted varying effects of vapor quality on heat transfer and developed a new correlation for flow boiling predictions.

Mancin et al. [41] examined how mass flow rate, heat flux, and vapor quality affect the heat transfer coefficient for R134a and R1234ze(E) in 5 PPI copper foam (0.93 porosity) at heat fluxes of 50 and 100 kW/m^2 and vapor qualities from 0.2 to 0.95. In turn, Zhu et al. [52] studied how metal foam packing affects flow boiling heat transfer in 7.9 mm ID horizontal tubes. They found that 5 PPI and 10 PPI foams improved the heat transfer coefficient by up to 111% and 139%, respectively. The enhancement was mainly due to increased heat transfer area and promotion of annular flow, especially at lower mass fluxes, with up to 2.4 times higher heat transfer coefficients compared to smooth tubes. They developed a method to correlate heat transfer coefficients for refrigerant boiling in metal-foam-filled tubes.

Conversely, Bamorovat Abadi et al. [43] examined flow boiling in 4 mm ID mini tubes packed with 20 and 30 PPI metal foams (porosity 0.9). They found that existing correlations for heat transfer were inadequate for foam-filled tubes and introduced an improvement factor of up to 3.2, demonstrating significant heat transfer enhancement. They also developed new correlations for the boiling heat transfer coefficient in packed tubes.

Gao et al. [53] introduced an open-cell metal foam mini-channel evaporator (OMFME) to enhance heat transfer in electronics cooling applications, using R134a as the working fluid. The study demonstrated that the OMFME achieved up to a 1.5 times higher heat transfer coefficient (HTC) compared to a conventional mini-channel evaporator (ME). The results showed that the HTC typically rose with higher vapor quality and heat flux, while changes in mass flow rate had only a small impact.

Samir and Hussain [42] developed correlations for predicting the Nusselt number in R-134a convective boiling in vertical tubes with copper foam. Metal foams increased the heat transfer coefficient by 270–310% (80 PPI) and 130–220% (40 PPI) compared to a smooth tube.

In a related study, Azizifar et al. [44] studied heat transfer in a horizontal steel pipe with copper foam (porosity 0.8, 10 PPI) during subcooled flow boiling of water. The metal foam increased the heat transfer coefficient by up to 580% and improved the thermal performance index by 22%.

Similarly, Weise et al. [45] and Haertlé [49] analyzed the impact of open-cell copper foam (10 and 20 PPI, 0.9 porosity) on flow boiling heat transfer in 14 mm horizontal tubes using CO_2, with heat fluxes up to 65 kW/m^2. They identified wetting and convective heat transfer as key performance factors and developed a predictive model for heat transfer in tubes with porous packing.

Liaw et al. [50] studied subcooled flow boiling in helical tubes with copper foam (80–95% porosity, 5, 6, and 10 PPI) and developed a 3D pore-scale model. They assessed the effects of inlet temperature, mass flux, and foam properties, deriving empirical Nusselt number correlations. Their findings show that porosity and pore density significantly affect heat transfer, with foam in the outer half of the tube yielding slightly better performance.

In turn, Li et al. [44] investigated flow boiling of R141b in micro-channels (Dh = 2.5 mm) with copper foam (20 PPI, 0.95 porosity). They observed a 2.5 to 3-fold heat transfer improvement compared to empty channels and proposed a new heat transfer correlation using a Gaussian function.

Bamorovat Abadi and Kim [47] examined boiling heat transfer in plate heat exchangers filled with metal foam using R245fa/R134a and pure R245fa. They found that 20 PPI foam increased the heat transfer coefficient by up to 2.3 times compared to conventional evaporators, while 30 PPI and 60 PPI foams enhanced it by up to 2 and 1.3 times, respectively.

Kouidri and Madani [19] studied heat transfer in a vertical compact heat exchanger filled with various metal foams (20 PPI, 93% porosity) during flow boiling of n-pentane. They found that copper foam improved heat transfer by 1.3 to 3 times, while NiFeAlCr and Inconel foams were less effective and sometimes worsened performance compared to copper foam.

Hu et al. [54,55] examined the effect of surface wettability on flow boiling heat transfer in metal foam-filled tubes. Hu et al. [54] found that hydrophilic surfaces decreased the heat transfer coefficient by 2–18%, while hydrophobic surfaces increased it by 6–30% with R134a in copper tubes with 10–40 PPI foams, and developed heat transfer correlations. Hu et al. [55] confirmed these results with R1234ze(E), showing hydrophilic surfaces reduced heat transfer by 7–13% and hydrophobic surfaces improved it by 3–8%, and introduced new heat transfer correlations for differences in metal foam surface wettability.

A review of the literature shows that high-porosity metal foams significantly enhance convective boiling heat transfer by increasing surface area, generating turbulence, and improving wetting, which reduces film thickness and boosts vapor-phase heat transfer. Theoretical and simulation studies confirm these benefits, leading to higher Nusselt numbers, disrupted thermal boundary layers, and reduced thermal resistance, outperforming traditional heat exchangers like shell-and-tube, finned, and plate designs.

Furthermore, metal foams, with their complex matrix and high specific surface area, show significant potential for enhancing condensation heat transfer by improving surface wetting and facilitating condensate removal, as evidenced by Wang et al. [56], Shi et al. [57], and Shenming et al. [32]. Wang et al. [56] studied R134a condensation in horizontal tubes with metal foam, finding that while foam tubes improved heat transfer, they also increased pressure drop. Shi et al. [57] demonstrated that annular metal foams (10–20 PPI) enhance water vapor condensation, with 10 PPI foam offering the best performance, achieving 1.3 times higher efficiency than micro-fin tubes. Additionally, Shi et al. [58] found that hydrophobic metal foams further improved heat transfer, with a 10 PPI foam reaching an HTC of 30,153 $W/m^2 \cdot K$ under specific conditions.

The foams are increasingly utilized in chemical reactors specifically designed to support heterogeneously catalyzed multiphase reactions involving both gaseous and liquid substrates. They serve simultaneously as both a filler and a catalyst support, providing an effective alternative to conventional packing materials [59]. By improving mass transport and increasing the active surface area, open-cell metal foams significantly enhance the performance of devices used for sensing, chemical conversion, and biochemical applications [60,61], and at the same time improve heat transfer for endothermic or exothermic processes.

Reactions occurring under non-boiling gas–liquid two-phase flow conditions include catalytic hydrogenation, where hydrogen is introduced to an organic molecule in the presence of a catalyst, such as palladium, platinum, or rhodium. Hydrogenation plays a crucial role in various industries, including food production, petrochemical refining, and pharmaceuticals, by enabling the synthesis of a wide range of organic chemicals (i.e., solvents, cosmetics, food additives, chemical reagents, fuel additives, lubricants, plastics). A notable example of hydrogenation is the conversion of nitrobenzene to aniline, catalyzed by palladium at 50 °C [62]. Other significant reactions include the hydrogenation of furan to tetrahydrofuran (THF) and maleic acid to succinic acid, with reaction times for gas–liquid hydrogenation of cyclohexene using a porous silicon-supported integrated catalyst

often being comparable to or better than those of traditional packed-bed reactors [63]. Traditionally, many hydrogenation processes have been conducted in batch reactors, leading to lower yields and selectivity. In contrast, continuous flow technology in tubular reactors is gaining popularity for its safety and efficiency, as seen in the continuous production of hexafluoroisopropanol (HFIP), an essential intermediate for the inhalation anesthetic sevoflurane, produced via catalytic hydrogenation of hexafluoroacetone (HFA) [64].

Based on a thorough review of the literature, it is evident that extensive investigations have been conducted on one-component two-phase flow under boiling and condensation conditions in pipes and channels packed with open-cell metal foams. In turn, research on two-phase non-boiling two-component gas–liquid flow in tubular reactors, conducted in the context of hydrogenation reactions, has primarily focused on the analysis of flow hydrodynamics and mass transfer phenomena.

To the best of the authors' knowledge, no studies have specifically addressed convective heat transfer models for two-component, gas–liquid non-boiling flow through pipes packed with open-cell metal foams. The limited information on gas–liquid flows in open-cell metal foams, especially outside of boiling refrigerant scenarios, and the lack of predictive methods for heat transfer coefficients, significantly hinder the design and optimization of equipment utilizing metal foams (e.g., tubular flow reactors), which are of great industrial importance. To address this gap, experimental studies were conducted to investigate heat transfer conditions in two-phase gas–liquid flow through channels packed with metal foams. The focus was on evaluating factors influencing heat transfer, including fluid properties, phase velocities, volume fractions in the two-phase mixture, and the impact of flow patterns on heat transfer from the channel wall to the two-phase mixture through the metal foam. Additionally, the effect of foam parameters on these phenomena was examined. It was also considered essential to identify an appropriate method for predicting the heat transfer coefficient in gas–liquid two-phase flow through channels filled with open-cell metal foams.

2. Test Stand, Scope and Methodology of the Research

The direct objective of the experimental studies was to evaluate heat transfer from the heated channel wall, filled with open-cell metal foam, to the gas–liquid two-phase mixture flowing through the channel, based on the temperature increase of the mixture. In the research, air, demineralized water, and Velol-9Q machine oil were used as fluids to create gas–liquid two-phase mixtures. To meet the study's objectives, the liquids were selected for their differing physical and thermal properties. The oil has a significantly lower density compared to water, more than twice lower specific heat and surface tension, and several times lower thermal conductivity. Moreover, it has relatively low viscosity, which at room temperature is about 9 times higher than that of water. Using oil with higher viscosity would have limited the study to laminar flow, as liquid flow through metal foams is characterized by relatively high flow resistance. The use of two different liquids allowed for variation in the physical properties of the generated two-phase mixtures. The experiments were conducted using a setup (Figure 1) with the main component being a heated horizontal channel fully filled with aluminum alloy foam. Three different types of foams were used, with each type having its own independent channel. All foams featured similar geometric cellular structures and comparable porosity ϕ. However, they differed in pore density (20, 30, and 40 PPI), as well as in cell size d_c and pore size d_p. In the context of metal foams, the term "pore" refers to the "window" connecting adjacent cells. The foams used in the study had cell sizes that differed by 53%, with a corresponding difference in thermal conductivity of 26%. Furthermore, the similar porosity of the foams allowed for a clear assessment of the impact of cell size on the thermal and flow phenomena under investigation. The aluminum alloy used for the 40 PPI foam exhibits higher thermal conductivity k_s compared to the material of the foam skeletons for 20 and 30 PPI foams. The key parameters characterizing the foams are summarized in Table 1. The methods for

determining cell diameter and pore size, as well as permeability and inertia coefficient, are described in ref. [65].

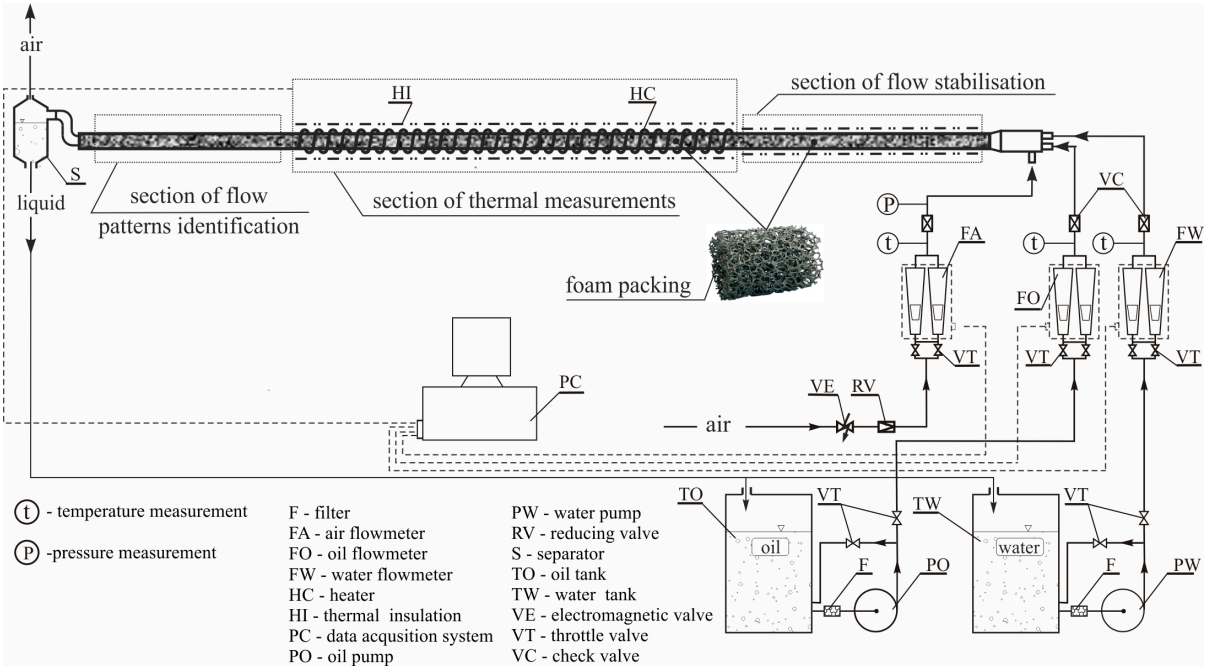

Figure 1. Diagram of the experimental setup.

Table 1. Foam specifications.

Foam 20		
alloy	AlSi7Mg	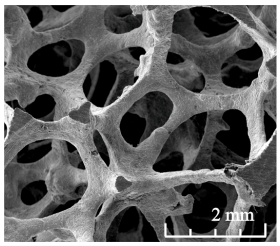
pore density, ω [PPI]	20	
porosity, ϕ	0.934	
cell diameter, d_c [m]	$3.45 \cdot 10^{-3}$	
pore diameter, d_p [m]	$1.09 \cdot 10^{-3}$	
thermal conductivity, k_s [W/(m·K)]	150.4	
permeability, K [m^2]	$1.274 \cdot 10^{-7}$	
inertial coefficient, β [m^{-1}]	154.1	
Foam 30		
alloy	AlSi7Mg	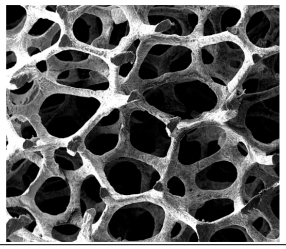
pore density, ω [PPI]	30	
porosity, ϕ	0.943	
cell diameter, d_c [m]	$2.25 \cdot 10^{-3}$	
pore diameter, d_p [m]	$0.71 \cdot 10^{-3}$	
thermal conductivity, k_s [W/(m·K)]	150.4	
permeability, K [m^2]	$0.659 \cdot 10^{-7}$	
inertial coefficient, β [m^{-1}]	191.1	
Foam 40		
alloy	Al 6101	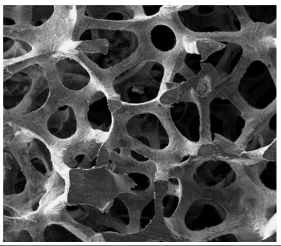
pore density, ω [PPI]	40	
porosity, ϕ	0.929	
cell diameter, d_c [m]	$2.39 \cdot 10^{-3}$	
pore diameter, d_p [m]	$0.82 \cdot 10^{-3}$	
thermal conductivity, k_s [W/(m·K)]	189.4	
permeability, K [m^2]	$0.700 \cdot 10^{-7}$	
inertial coefficient, β [m^{-1}]	277.0	

The test channel was constructed as an aluminum pipe with an internal diameter of 0.02 m and a total length of 2.61 m. At the inlet of the channel, a flow stabilization section, 0.92 m in length, is included to ensure consistent flow conditions. The central part of the channel, extending 1.27 m, serves as the measurement section where variations in the temperature and pressure of the fluids were recorded. In this section, the channel is heated externally using a resistance heater wrapped around it, with a nominal power of 4400 W. The study utilized commercially manufactured aluminum foams from m-pore (20 and 30 PPI) and ERG Aerospace Corporation, in the form of plates with a thickness of 30 mm. The foams were placed inside the channel as cylindrical inserts with a diameter equal to the inner diameter of the channel, which is 20 mm, and a length of 30 mm. The inserts were cut using electrical discharge machining. To ensure effective heat transfer from the heated channel wall to the foam structure, the inserts were bonded to the surface of the tube using a high-conductivity adhesive based on aluminum powders. For this purpose, it was necessary to longitudinally cut the channel into two parts, which were then tightly joined by soldering after the foam was inserted.

In the heated section of the channel, the metal foam was bonded to the pipe using a thermally conductive epoxy-aluminum adhesive to reduce the thermal resistance between the foam structure and the channel wall. The measurement section was thermally insulated with 0.07 m thick mineral wool. A schematic of the measurement section, including the location of the measurement equipment, is shown in Figure 2.

During the experiments, temperatures of the fluids and the channel wall were measured using Type K thermocouples with a diameter of 1 mm. Temperature measurements were conducted at four transverse sections along the measurement section (see Figure 2, sections I, II, III, IV). Sections I and IV were located 160 mm from the start and end of the heated section, respectively. This distance is sufficient to establish a steady-state temperature profile of the fluid.

According to the literature, the temperature profile in horizontal flow through metal foams typically stabilizes over a length equal to 3–4 times the channel's cross-sectional dimension (160 mm is eight times the diameter of the channel used). In each of the four transverse sections (I–IV), eight thermocouples were installed. The sensing tips of five thermocouples were positioned inside the channel at various distances from its center in the vertical plane, while the tips of three additional thermocouples were placed 0.5 mm from the inner surface of the pipe, within the channel wall. The temperature of the wall, like that of the fluids, was measured at the bottom, middle, and top sections of the channel. This setup allowed for the consideration of the vertical temperature profile's influence on the average temperature values. The thermocouples were connected to eight-channel measurement modules, which were equipped with a reference temperature stabilization and correction system. These modules, along with a computer, formed a data acquisition system that enabled real-time observation and recording of temperature changes simultaneously at all measurement points. Before the experiments began, the temperature measurement system was calibrated. After calibration, all thermocouple readings were within ± 0.2 K of the reference temperature.

The pressure drop of the gas–liquid mixture through the measurement section, along with the overpressure at the section's inlet, were also measured. Knowledge of these parameters was crucial for determining the properties of the air and flow patterns. Pressure measurements were conducted using a set of four piezoresistive differential pressure sensors and one absolute pressure sensor. The specification of the measurement apparatus is provided in Table 2. The measurement uncertainty of the apparatus was evaluated in accordance with the guidelines outlined in the Guide to the Expression of Uncertainty in Measurement [66]. The relative standard uncertainty of the measured quantity x is described by Equation (1).

$$\frac{u(x)}{x} = \left(\left(\Delta_d x^2 + \Delta_e x^2 \right) / 3 \right)^{0.5} \quad (1)$$

$\Delta_d x$ in Equation (1) represents the uncertainty due to calibration (or reference), and $\Delta_e x$ denotes the experimenter's uncertainty. The calibration uncertainties were determined based on linear regression of the calibration results. The experimenter's uncertainty, $\Delta_e x$, was considered to be the value of the last significant digit in the measurement result. Table 2 provides the maximum relative uncertainties (expressed as percentages) for the measurement sensors.

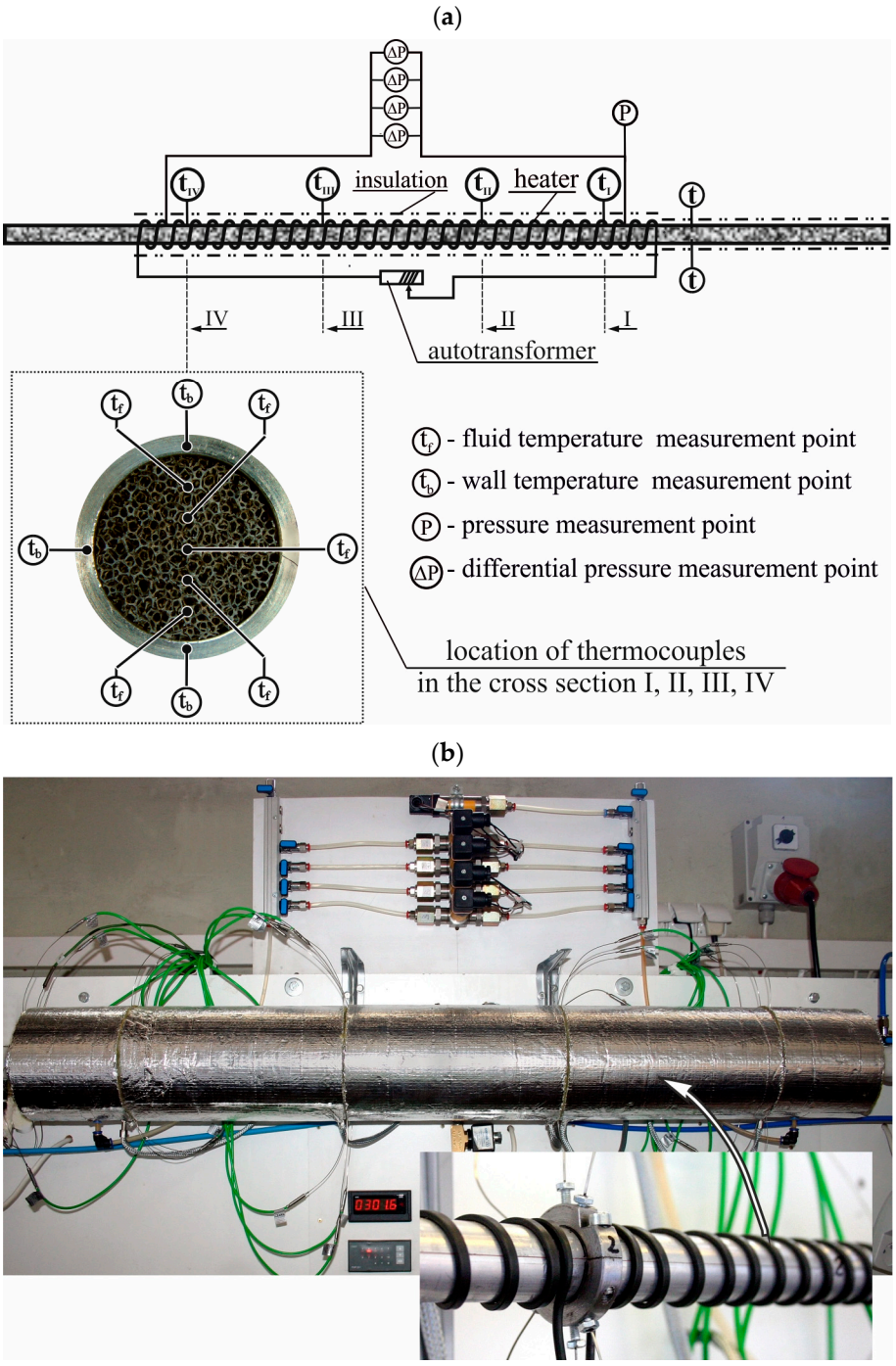

Figure 2. Measurement section. Scheme (**a**), real view (**b**).

Table 2. Specification of the measurement equipment.

Measurement	Measurement Range	Sensor Accuracy Class *	Relative Uncertainty **
Air flow rate, [m^3/s]	$0–3.33 \cdot 10^{-4}$ $3.33 \cdot 10^{-4}–3.33 \cdot 10^{-3}$	0.2 0.3	2.4% 1.7%
Water flow rate, [m^3/s]	$2.5 \cdot 10^{-7}–1.17 \cdot 10^{-5}$ $8.33 \cdot 10^{-6}–8.33 \cdot 10^{-5}$	1.0 1.0	4.1% 4.2%
Oil flow rate, [m^3/s]	$3.33 \cdot 10^{-7}–6.67 \cdot 10^{-5}$	2.0	6%
Differential pressure, [Pa]	$(0–2) \cdot 10^3$ $(2–10) \cdot 10^3$ $(10–50) \cdot 10^3$ $(5–150) \cdot 10^3$	1.6 0.4 0.25 0.25	3.7% 1.2% 0.7% 0.4%
Pressure, [Pa]	$(0–600) \cdot 10^3$	0.25	0.3%
Temperature, [°C]	(0–100)	$\Delta_d x = 0.2$ K **	0.3%

* declared by the producer in relation to the measuring range. ** refers to the measured value determined based on calibration.

Simultaneously with the heat transfer investigations, the identification of flow structures developing within the channel was conducted, enabling an assessment of their potential impact on heat transport. Due to the need to observe flow structures, the final section of the channel, measuring 0.42 m in length (beyond the measurement section), was constructed from transparent acrylic glass. The identification of flow patterns was conducted concurrently through visual observations made during the experiment, supplemented by high-resolution photographs of the structures taken with a camera. Additionally, an algorithm for identifying flow structures based on fractal analysis of pressure drop fluctuations, which were recorded in real time throughout the experiment, was employed. The methodology for identifying flow structures based on the fractal analysis of pressure drop fluctuations is thoroughly described in the work of Broll and Dyga [67].

The experiments were conducted in measurement series where a constant liquid flow rate was maintained while gradually increasing the air flow rate. As the flow rate of the fluids increased, the heating power q_h was also increased to ensure that the temperature of the mixture rose by at least 10 K. The heating power was adjusted by varying the voltage.

The experiments were conducted over a relatively wide range of fluid flow rates, which allowed for a broad diversity of flow structures and ensured that both laminar and turbulent flow regimes were achieved, as demonstrated in previous studies [65,68]. The main parameters characterizing the flow conditions are presented in Table 3.

Table 3. Conditions for conducting experimental research.

Fluid Flow Parameters				
Fluid, *f*	**v_{sf}, m/s**	**g_f, kg/(m²·s)**	**Re_f *, -**	**ε_f/x **, -**
air, *a*	0.060–2.664	0.07–2.93	42–2502	0.488–0.988
water, *w*	0.006–0.063	5.56–62.57	106–1487	0.001–0.361
oil, *o*	0.006–0.063	4.86–53.39	17–253	
Properties of oil Velol-9Q				
density ρ, kg/m^3	$\rho = 875.03 - 0.783t + 0.0012t^2$			
viscosity μ, Pa·s	$\mu = 0.1172t^{-0.865}$			
conductivity k, W/(m·K)	$k = 0.1232–2.55 \cdot 10^{-4}t + 1.25 \cdot 10^{-6}t^2$			
specific heat c, J/(kg·K)	$c = 1767 + 4.122t + 0.0016t^2$			

* determined using Equation (16). ** at the inlet to the channel.

It was assumed that similar hydrodynamic conditions would be achieved for both two-phase mixtures when flowing through each of the three foams. The primary criteria for the flow were the superficial phase velocities v_{sf}, described by Equation (2), which are

understood as the mean velocities of the fluids in the channel, calculated while neglecting the presence of the second fluid and foam.

$$v_{sf} = V_f \frac{4}{\pi d^2} \tag{2}$$

3. Examination of Results

The heat transfer analysis was conducted based on the thermal balance of the fluids within the heated section of the channel, confined to the area between cross-sections I and IV (as indicated in Figure 2). These cross-sections are thus treated as the inlet and outlet of the channel, respectively. The heat absorbed by the gas–liquid mixture from the channel wall and the foam skeleton is equivalent to the sum of the heat fluxes absorbed by the gas and the liquid phases.

$$Q_{tp} = Q_g + Q_l \tag{3}$$

The heat absorbed by the gas and liquid is described by the following equations, respectively

$$Q_g = m_g\left(i_{g,out} - i_{g,in}\right), \tag{4}$$

$$Q_l = m_l(i_{l,out} - i_{l,in}). \tag{5}$$

The initial and final enthalpy values of the fluids $i_{f,in}$ and $i_{f,out}$ were determined based on the average fluid temperatures at the inlet and outlet of the channel, $\bar{t}_{in}$ and $\bar{t}_{out}$, respectively. The average values were determined based on the readings from all thermocouples measuring the fluid temperatures within the specified cross-section ("in" or "out").

It was assumed that in the heated section of the channel, the temperatures of the gas and liquid are equal, i.e., in the air–water flow, $t_g = t_w = t_{tp}$, and in the air–oil flow, $t_g = t_{ol} = t_{tp}$. This assumption was experimentally validated for stratified flow. In this type of flow, the thermocouple positioned in the lower part of the channel was exclusively exposed to the liquid phase, while the thermocouple in the upper part of the channel was in contact solely with the gas phase and therefore measured only the air temperature. The results indicate that the temperatures of air and water equilibrate in the channel before reaching the heated measurement section. The differences between the temperature readings of the thermocouples for both phases were within the measurement error margin. In the case of non-stratified flows, where more intensive mixing of the fluids occurs, temperature equalization between the fluids is even more likely. This is particularly true considering that the initial temperatures of the air and the liquid differed by no more than 2–3 K.

The enthalpy of the liquid (i_l) is described by Equation (6).

$$i_{l,in(out)} = c_l \bar{t}_{tp,in(out)}, l \equiv w, ol. \tag{6}$$

When calculating the enthalpy of air, its humidity Y was taken into account in Equation (7).

$$i_{g,in(out)} = c_g \bar{t}_{tp,in(out)} + (c_v \bar{t}_{tp,in(out)} + r)Y. \tag{7}$$

In the case of air–oil flow, the humidity of the air was measured before its entry into the measurement channel. However, for air–water flow, the enthalpy of the air was calculated based on the assumption of air saturation. Due to the co-current flow of air and water, the air progressively becomes saturated with water vapor. Given the relatively long flow stabilization section, it was assumed that saturation is achieved before entering the measurement section and is maintained throughout its length. The heat transfer coefficient is described by Equation (8).

$$h_{tp} = \frac{Q_{tp}}{S\left(\overline{t_b} - \overline{t_{tp}}\right)}. \tag{8}$$

In (8), the surface of the channel wall (between sections I and IV) was taken as the heat transfer surface S. The difference between the temperature of the gas–liquid mixture and the wall temperature varies along the flow path. Therefore, the average value of this temperature difference $\overline{(\overline{t_b} - \overline{t_{tp}})}$ was determined through approximate integration, as described by Equation (9).

$$\overline{(\overline{t_b} - \overline{t_{tp}})} = \frac{1}{L_{VI} - L_I} \int_{L_I}^{L_{IV}} (\overline{t_b} - \overline{t_{tp}}) dL. \tag{9}$$

The uncertainty in the value of the heat transfer coefficient $u(h)$ was assessed based on the principle of propagating uncertainties from direct measurements:

$$u(h) = \sqrt{\sum_i \frac{\partial h}{\partial x} u^2(x_i)}, \tag{10}$$

where the uncertainty of directly measured quantities $u(x)$ is described by Equation (1).

Figures 3–6 present selected results from the experimental analysis, which are representative of all studied cases of air–water and air–oil flow through the three types of foam. In the air–water mixture flow, the heat transfer coefficient increases with rising fluid velocities (see Figure 3). The effect of increasing the water flow rate on the heat transfer coefficient is particularly pronounced. For example, a tenfold increase in water velocity, from 0.006 to 0.061 m/s, leads to an approximately twofold increase in the heat transfer coefficient. In contrast, a multiple increase in air velocity results in only a modest rise in the heat transfer coefficient, typically on the order of several percent. Particularly at higher air velocities, the impact of this phase on the heat transfer coefficient is relatively minor. For air velocities around 0.5 m/s, a nearly linear relationship between the heat transfer coefficient and air velocity becomes apparent. In the majority of the investigated cases, the heat transfer intensity in the two-phase flow was higher than in the single-phase flow of fluids transported through the channel at the same superficial velocity. The introduction of even a small amount of air into the water flow results in an increase in the heat transfer coefficient by several to tens of percent, as illustrated in Figures 3 and 5, with air velocity changing from v_{sg} = 0 to v_{sg} = 0.07 m/s. If the introduction of air into the liquid induces a plug flow regime, the increase in the heat transfer coefficient can reach approximately 25%. Further increases in the air flow rate lead to a monotonic rise in the heat transfer coefficient due to the growing turbulence in the flow. Deviations from this trend are observed when transitioning from plug flow to stratified flow, where a decrease in the heat transfer coefficient occurs despite an increase in gas velocity.

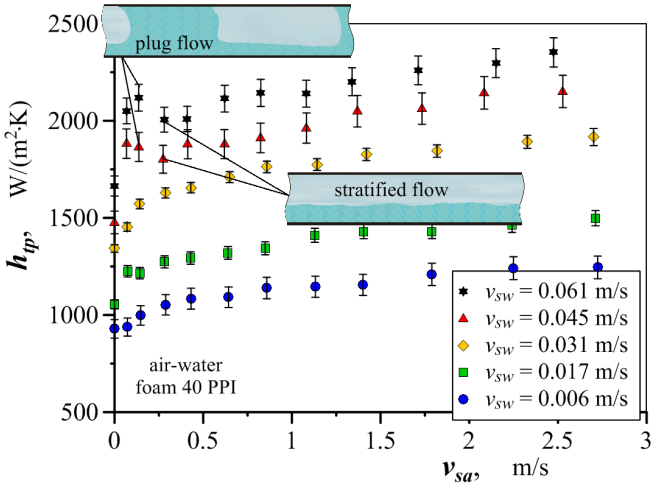

Figure 3. Variation in the heat transfer coefficient for air–water flow through a 40 PPI foam-filled channel.

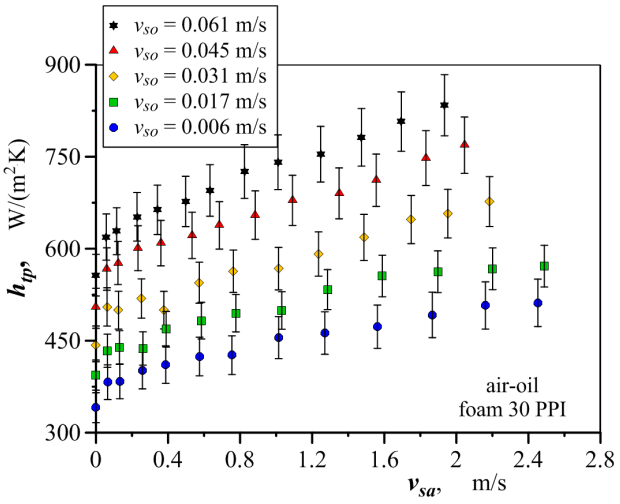

Figure 4. Variation of the heat transfer coefficient for air–oil flow through a channel filled with 30 PPI foam.

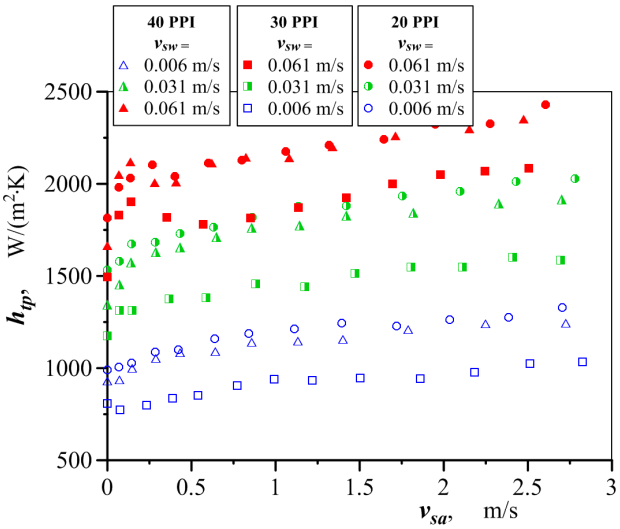

Figure 5. Heat transfer coefficient for air–water flow through 20, 30, and 40 PPI foams.

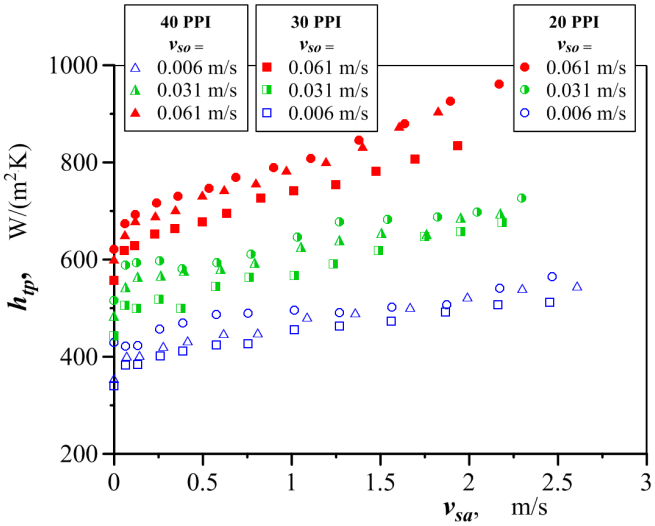

Figure 6. Heat transfer coefficient for air–oil flow through 20, 30, and 40 PPI foams.

Transition from plug flow to stratified flow results in a reduction in the contact area between the water and the channel wall, as well as the foam. The heat transfer intensity between the water and the wall or foam is significantly greater than between the air and the solid materials. Therefore, in a two-phase flow, a reduction in the liquid contact with the wall leads to a decrease in the heat transfer coefficient h_{tp}. Such singularities related to changes in flow structures are typical of multiphase flows, although they primarily pertain to flow resistance and the volumetric fractions of phases within the mixture [69–71]. However, with respect to heat transfer in gas–liquid flows through metal foams, these phenomena have not been previously documented. In the air–oil flow studies, a similar trend in the heat transfer coefficient was recorded, specifically an increase in h_{tp} with rising velocities of both fluids, with air having a lesser impact compared to oil. The results of these studies are presented in Figure 4. In the air–oil flow, the heat transfer coefficient is more than twice as low compared to the air–water flow under identical conditions, specifically at the same superficial phase velocities. The higher viscosity of the oil leads to reduced turbulence compared to water, which is the primary reason for the lower intensity of heat transfer in flows involving oil.

In the case of air–oil flow, the reduction in the heat transfer coefficient observed in air–water flow during the transition from plug flow to stratified flow was not evident. The air–oil flow exhibited a greater diversity of flow structures. In the air–water flow studies, stratified flow accounted for over 70% of all observed flow cases. During the air–oil flow experiments, slug and churn flows were frequently observed under conditions where stratified flow occurred in the air–water flow. In slug and churn flows, similarly to plug flow, the liquid wets a large part of the heat exchange surface. Therefore, the transition from plug flow to another type of flow, as long as it is not stratified, does not result in a significant change in the heat transfer coefficient.

The heat transfer coefficient exhibits varying values under identical flow conditions across different types of foam. This variability is likely attributable to differences in the geometric structure and thermal conductivity of the foams. As illustrated in Figures 5 and 6, the highest heat transfer coefficients, for both air–water and air–oil flows, were observed through the 20 PPI foam, whereas the lowest values were recorded for the 30 PPI foam.

The 20 PPI foam, characterized by the thickest fiber structure, exhibits the lowest resistance to heat transfer from the wall to the foam. Considering the specific surface area of the foam, the heat transfer coefficient should be higher for flow through a channel filled with 30 PPI foam compared to 20 PPI foam, as 30 PPI foam has a larger specific surface area. However, the contrary observation in the experiments indicates that heat transfer in channels filled with foam primarily occurs between the channel wall and the fluid, with the foam playing a lesser role in heat transfer. The heat transfer coefficient for flow through 40 PPI foam falls between the values observed for 20 PPI and 30 PPI foams. The 40 PPI foam has geometric parameters similar to those of the 30 PPI foam but features a 26% higher thermal conductivity of the foam material. Since some of the heat is transferred via conduction through the channel wall–foam skeleton–fluid system, the thermal conductivity of the foam skeleton can influence the heat flux absorbed by the fluid, and consequently, the experimentally determined heat transfer coefficient. In the case of air–oil flow, the impact of the foam on the heat transfer coefficient is also noticeable but to a lesser extent.

4. Model for Calculating the Heat Transfer Coefficient

Due to the lack of methods for calculating the heat transfer coefficient in non-boiling two-component gas–liquid flows through metal foams, an analysis was conducted to assess the applicability of methods designed for two-component gas–liquid flows in empty channels. This assessment also considered methods developed for boiling flows through channels filled with metal foams (Table 4). The analysis focused on the methods proposed by Bamorovat Abadi et al. [43], Ghajar [72], Khoze et al. [73], Kim et al. [74], Nada [75], Rezkallah et al. [76], Samir et al. [77], and Zhu et al. [40]. The selection of these methods was influenced by the fact that they are designed for horizontal channel flows, and their

applicability is at least partially aligned with the experimental conditions described in this study.

Table 4. Methods for calculating the heat transfer coefficient in gas–liquid flow.

Source	Correlation Describing Nu_{tp}, h_{tp}	Main Complementary Variables	System and Range of Parameter Changes
Two-component gas–liquid flow in an empty channel			
Ghajar [72]	$\frac{h_{tp}}{h_l} = (1-R_g)\left[1+65\left(\frac{x}{1-x}\right)^{0.25}\left(\frac{R_g}{1-R_g}\right)^{0.25}\cdot\left(\frac{Pr_g}{Pr_l}\right)^{0.33}\left(\frac{\mu_g}{\mu_l}\right)^{0.33}e^{1.4\theta}\right]$	laminar flow $h_l = 1.86\left(Re_l\, Pr_l\frac{d}{L}\right)^{0.33}\left(\frac{\mu_{lb}}{\mu_l}\right)^{0.14}\frac{k_l}{d}$ turbulent flow $h_l = 0.027\, Re_l^{0.4}\, Pr_l^{0.33}\left(\frac{\mu_{lb}}{\mu_l}\right)^{0.14}\frac{k_l}{d}$ $Re_l = \frac{4m}{\pi\sqrt{1-R_g}\mu_l d}$	air–water flow in a horizontal channel $Re_l = 2836-8298$
Khoze et al. [73]	$Nu_{tp} = 0.26\, Re_g^{0.2}\, Re_l^{0.55}\, Pr_l^{0.4}$	$Re_l = \frac{\rho_l d v_{sl}}{\mu_l}$; $Re_g = \frac{\rho_g d v_{sg}}{\mu_g}$	gas–liquid flow in rectangular channels air–water, air–diphenyloxide, air–polymethylsiloxane $Re_l = 3.5-210$ $Re_g = 4000-37000$
Kim et al. [74]	$\frac{h_{tp}}{h_l} = (1-R_g)\left[1+2.86\left(\frac{x}{1-x}\right)^{0.42}\left(\frac{R_g}{1-R_g}\right)^{0.35}\cdot\left(\frac{Pr_g}{Pr_l}\right)^{0.66}\left(\frac{\mu_g}{\mu_l}\right)^{-0.72}e^{1.4\theta}\right]$	laminar flow $h_l = 1.86\left(Re_l\, Pr_l\frac{d}{L}\right)^{0.33}\left(\frac{\mu_{lb}}{\mu_l}\right)^{0.14}\frac{k_l}{d}$ turbulent flow $h_l = 0.027\, Re_l^{0.4}\, Pr_l^{0.33}\left(\frac{\mu_{lb}}{\mu_l}\right)^{0.14}\frac{k_l}{d}$ $Re_l = \frac{4m}{\pi\sqrt{1-R_g}\mu_l d}$	air–water slug, bubbly-slug, bubbly-slug-annular flow in a horizontal channel $Re_l = 2468-35503$
Nada [75]	$\frac{Nu_{tp}}{Nu_l} = 1-0.2314\, Re_l^{-0.77}\left(10^{-5}Re_g^2 - Re_g\right)$	$Nu_l = \frac{(f/8)(Re_l-1000)Pr_l}{1+12.7\sqrt{f/8}\left(Pr_l^{0.66}-1\right)}\cdot\left(1+(d/L)^{0.66}\right)$ $f = (1.82 log Re_l - 1.64)^{-2}$	air–water slug/stratified/annular flow in a horizontal empty channel $Re_l = 7000-17800$ $Re_g = 1000-7000$
Rezka-llah et al. [76]	$\frac{h_{tp}}{h_l} = (1-R_g)^{-0.9}$	$h_l = 1.86\left(Re_l\, Pr_l\frac{d}{L}\right)^{0.33}\left(\frac{\mu_{lb}}{\mu_c}\right)^{0.14}\frac{k_l}{d}$	air–water, air–glycerin water solution (58–42% by weight) air–silicone liquid bubble and slug flow
Single-phase vapor–liquid flow (boiling) in a empty channel/filled with metal foam channel			
Zhu et al. [40]	$h_{tp} = h_{empty} IF$ $h_{empty} = \frac{\theta_{dry}h_v + (2\pi-\theta_{dry})\left(h_{nb}^3+h_{cb}^3\right)^{1/3}}{2\pi}$ $IF = \left(\frac{A}{A_{ch}}\right)^{0.005129PPI+0.0447\theta_{dry}-5.796\frac{q}{ifcr}+0.3249}$	$h_v = 0.023\, Re_v^{0.8}\, Pr_v^{0.4}\frac{k_v}{d}$ $h_{cb} = 0.0133\, Re_l^{0.69}\, Pr_l^{0.4}\frac{k_l}{d}$ $h_{nb} = 55\, Pr_r^{0.12}(-\log P_r)^{-0.55}M^{-0.5}q^{0.67}$	boiling of R-410a in a copper foam-filled horizontal channel g_{tp} = 90–270 kg/(m^2·s)
Bamo-rovat Abadi et al. [43]	$h_{tp} = h_{empty} IF$ $h_{empty} = \left[(Fh_{cb})^2 + (Sh_{nb})^2\right]^{0.5}$ $IF = \left(\frac{A}{A_{ch}}\right)^{0.3253+4.3799\left(\frac{1-R_g}{4}\right)}$	$h_{cb} = 0.023\, Re_l^{0.8}\, Pr_l^{0.4}\frac{k_l}{d}$ $h_{nb} = 55\, Pr_r^{0.12}(-\log P_r)^{-0.55}M^{-0.5}q^{0.67}$ $F = \left[1+xPr_l\left(\frac{\rho_l}{\rho_v}\right)-1\right]^{0.35}$ $S = \left[1+0.55\, F^{0.1}\, Re_l^{0.16}\right]^{-1}$	boiling of R245fa in a copper foam-filled mini tube. annular flow, intermittent slug flow g_{tp} = 400–700 kg/(m^2·s)
Samir et al. [77]	$Nu_{tp} = 5.57\, Re_K^{0.631}\, Bo^{0.21}\, Pr^{0.74}$	$Re_K = \frac{\rho_l v_{sl}\sqrt{K}}{\mu_l}$; $Bo = \frac{q}{\rho_l v_{sl} r_l}$	boiling of R-134a in a copper foam-filled vertical channel g_{tp} = 8–40 kg/(m^2·s)

As shown in Figure 7, the calculated heat transfer coefficients deviate significantly from the experimentally determined values. The results of the statistical evaluation of the heat transfer coefficient calculation methods are presented in Table 5. The mean error and standard deviation were determined using the following equations:

$$\delta h_{tp} = \left|\frac{h_{tp,cal} - h_{tp,\exp}}{h_{tp,\exp}}\right| \cdot 100\% \tag{11}$$

$$RMS = \left[\frac{1}{n}\left(\sum_{i=1}^{n}\left(\frac{\left(h_{tp,cal}\right)_i - \left(h_{tp,exp}\right)_i}{\left(h_{tp,exp}\right)_i}\right)^2\right)\right]^{0.5}. \tag{12}$$

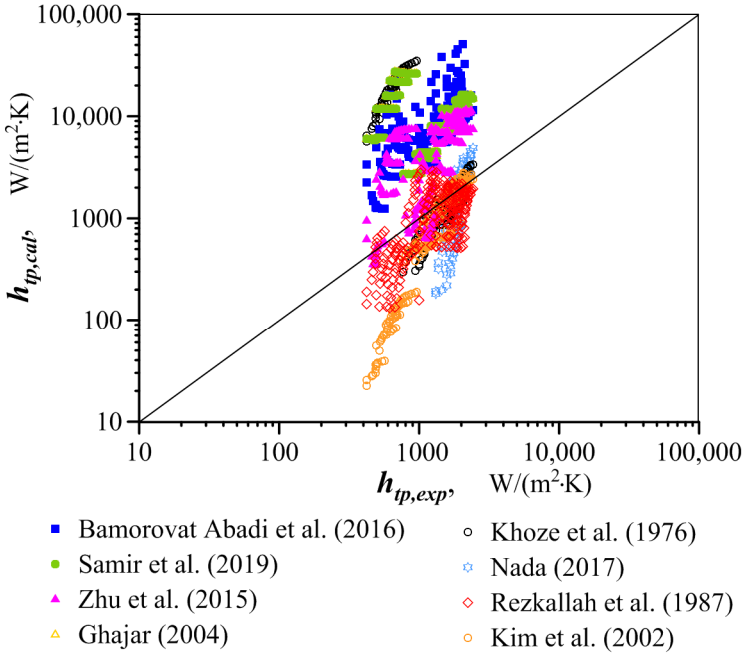

Figure 7. Comparison of heat transfer coefficient values calculated using literature methods with experimental data [40,43,72–77].

Table 5. Experimental conditions.

Method (Author)	Relative Error δh_{tp} [%]	Root Mean Square RMS [–]
	air–water/air–oil	air–water/air–oil
Bamorovat Abadi et al. [43]	659/658	7.05/8.68
Ghajar [72]	272/64	3.28/0.65
Khoze et al. [73]	24/2808	0.30/28.94
Kim et al. [74]	26/85	0.32/0.86
Nada [75]	44/–	0.50/–
Rezkallah et al. [76]	40/45	0.52/0.49
Samir et al. [77]	439/2359	4.62/24.93
Zhu et al. [40]	254/459	2.96/5.54

Relatively good agreement between experimental and calculated values was observed when applying methods developed for non-boiling flow in empty channels to the air–water flow. For the methods proposed by Khoze et al. [73] and Kim et al. [74], the mean calculation errors are 24% and 26%, respectively. However, for air–oil flow, the deviations between calculated and measured values are significantly larger and are considered unacceptable, particularly for the method proposed by Khoze et al. The Nada method is not applicable to laminar liquid flows (which encompass the entire range of air–oil mixture studies), as it results in negative values for the heat transfer coefficient. Additionally, the heat transfer coefficient during boiling through channels filled with foams reaches significantly higher values compared to non-boiling flows. Consequently, the heat transfer coefficients calculated using the methods proposed by Bamorovat Abadi et al. [43], Samir et al. [77], and Zhu et al. [40] are several times greater than the experimentally obtained values. It was identified that one of the main sources of significant calculation errors is the method used to define the factor IF, which quantifies the impact of the foam presence on the heat transfer coefficient.

The observed inaccuracies in calculating the heat transfer coefficient underscore the necessity for developing a specialized method tailored specifically for two-component non-boiling flows.

Observations of flow structures conducted during the experimental investigations indicate that in channels filled with foams, the flow structures are similar to those observed in gas–liquid flows through empty channels. In all cases, a clear separation between the gas and liquid phases was evident; the foam does not induce fragmentation of the fluids into small portions or their uniform dispersion throughout the channel volume. Therefore, it was assumed that the heat transfer coefficient in two-phase flow through foam-filled channels can be calculated based on a separated flow model, utilizing the heat transfer coefficients for the liquid (h_l) and gas (h_g) phases flowing independently. Analysis of the experimental data indicates that the heat transfer coefficient in gas–liquid flow exceeds the sum of the heat transfer coefficients for the gas and liquid in single-phase flows. The mutual interaction of the fluids in the combined flow ultimately leads to flow disturbances, which contribute to more intense heat transfer. Therefore, it was decided that the heat transfer coefficient in gas–liquid flow through a channel filled with metal foam can be described by the following equation:

$$h_{tp} = \left(h_l + h_g\right)\Phi_h. \tag{13}$$

In Equation (13), the parameter Φ_h, referred to as the enhancement factor, quantifies the intensification of heat transfer in the two-phase flow compared to single-phase flow.

The equal treatment of gas and liquid in this context arises from the fact that, over a broad range of flow conditions, the gas occupies a relatively large portion of the channel volume. Consequently, it limits the contact between the liquid and the channel wall, thereby influencing the heat transfer into the two-phase mixture to a greater extent than would be expected based solely on its mass fraction. At the same time, the liquid can absorb a significantly larger portion of the heat flux exchanged between the two-phase mixture and the channel wall, due to its high heat transfer coefficient and substantial heat capacity.

The collected experimental results indicate that the intensity of heat transfer in the gas–liquid two-phase flow through a channel filled with metal foam is primarily determined by the hydrodynamic flow conditions and the thermal properties of the fluids. The influence of the foam's geometric parameters is noticeably smaller. Similar conclusions were drawn by Dyga and Troniewski [78] in their studies of single-phase flow through metal foams. Therefore, it was assumed that the heat transfer coefficient for gas–liquid two-phase flow, described in Equation (13), can be determined using Equations (14) and (15) proposed in ref. [78].

$$Nu_f = CRe_f^{c_1} Pr_f^{c_2} Da_f^{c_3} \left(\frac{k_{eff}}{k_f}\right)^{c_4} \left(\frac{\mu_f}{\mu_{fb}}\right)^{c_5}, \tag{14}$$

$$h_f = \frac{Nu_f k_f}{d}, \text{where} : f \equiv l, g. \tag{15}$$

Basing Equation (14) on similarity modules allows for the consideration of the significant impact of flow conditions (Reynolds number) and fluid properties (Prandtl number) on heat transfer. While the influence of the foam's structural parameters on the heat transfer coefficient is less pronounced, it is still noticeable. The structural parameters of the foam were incorporated through the specifically defined hydraulic diameter, d_h, in the Reynolds number.

Considering that Equation (14), originally developed for single-phase flow, is to be applied to two-phase flow, it was assumed that the calculation of the heat transfer coefficient for both gas and liquid must account for the presence of the second phase in the channel. According to this assumption, the Reynolds number for each phase should be determined based on the mass flux density of the two-phase mixture, g_{tp}, and the following equation:

$$Re_f = \frac{g_{tp} d_h}{\eta_f}, \tag{16}$$

where the hydraulic diameter is described as

$$d_h = \frac{\phi d_p}{1-\phi}, \tag{17}$$

and incorporates the geometric parameters of the foam—pore diameter d_p and porosity φ. This method of defining the hydraulic diameter for flow through metal foams has been justified in the work by [57]. The influence of foam structure on heat transfer is also accounted for by introducing the Darcy number into Equation (14), based on the foam permeability K.

According to the recommendations of the authors in [79], the Darcy number should be determined using the following equation:

$$Da_f = \frac{K_f}{(0.5d)^2}. \tag{18}$$

Permeability is directly influenced by structural parameters of the foam, such as porosity, cell and pore size, the shape of the struts and nodes of the skeleton, and the surface condition of the skeleton.

The calculation of the heat transfer coefficient also takes into account the significance of the thermal conductivity of the skeleton. A specific characteristic of flow through a channel filled with metal foam is that heat exchange between the channel wall and the fluid flow occurs not only via convection but also through conduction in the foam–fluid system. The contribution of this form of heat transfer is incorporated using the effective thermal conductivity coefficient, described by the following equation:

$$k_{eff} = \phi k_f + 0.181(1-\phi)^{0.736} k_s, \tag{19}$$

which is based on the thermal conductivities of the skeleton k_s and the fluid k_f.

The constants present in Equation (14) are summarized in Table 6. Their values depend on the nature of the flow. The boundary for laminar flow is defined at Re = 1300 (according to Equation (16)).

Table 6. Constants in Equation (14).

	C	c_1	c_2	c_3	c_4	c_5
Laminar flow $Re_f \leq 1300$	3.9	0.3	0.2	0.1	0.4	0.14
Turbulent flow $Re_f > 1300$	1.9	0.4	0.3	0.1	0.33	0

Figure 8 shows the dependence of the enhancement factor on the flow conditions. The enhancement factor was determined based on Equation (13), using the experimentally measured heat transfer coefficient for the gas–liquid flow and the heat transfer coefficients for the gas and liquid calculated with Equation (14):

$$\Phi_{h,\text{exp}} = \frac{h_{tp,\text{exp}}}{h_{l,cal} + h_{g,cal}}. \tag{20}$$

To maintain clarity in the data presented in Figure 8, only selected results that are representative of all collected data are shown. The value of Φ_h is only slightly greater than one and exhibits minimal dependence on the flow conditions (fluid velocities). The enhancement factor increases slightly with liquid velocity and shows an almost linear dependence on air velocity.

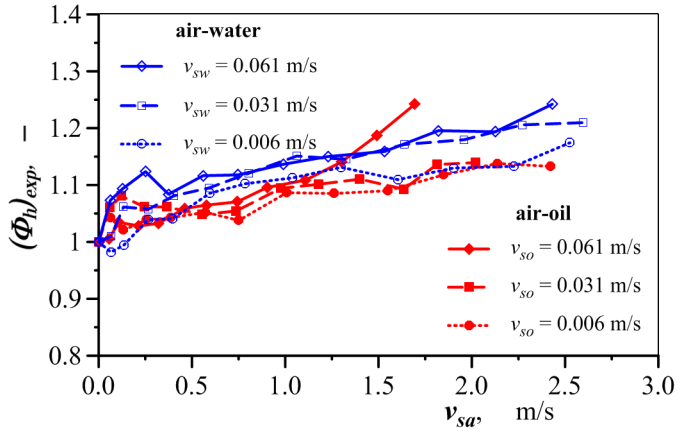

Figure 8. The heat transfer enhancement factor Φ_h.

The properties of the two-phase mixture do not exhibit a distinct influence on the heat transfer enhancement factor, as it shows similar values under analogous conditions for both air–oil and air–water flows. At equivalent flow velocities in both studied two-phase systems, the introduction of air into the liquid results in a comparable increase in the intensity of heat transfer. The functional relationship describing the heat transfer enhancement factor,

$$\Phi_h = 1 + 0.002 Re_l^{0.2} Re_g^{0.45} \left[\left(\frac{\mu_l}{\mu_w} \right) \left(\frac{\rho_w}{\rho_l} \right)^2 \right]^{0.33}, \quad (21)$$

was established considering the condition $\Phi_h \geq 1$ and the significance of flow conditions and phase properties. The values of the constant and the exponents in Equation (21) were determined based on correlation calculations. The comparison between heat transfer coefficients calculated using Equation (13) and the corresponding experimental data, presented in Figures 9 and 10, clearly indicates that the developed method accurately captures both the magnitude and the behavior of the heat transfer coefficient under the examined flow conditions.

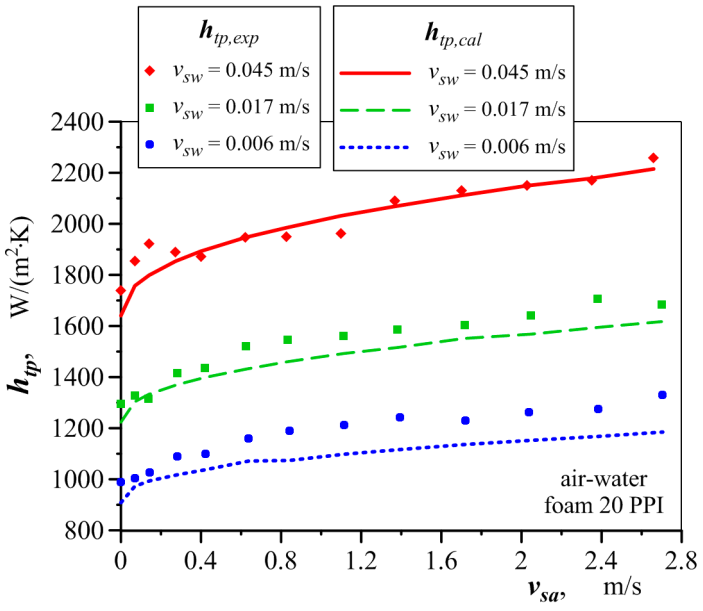

Figure 9. Comparison of experimental heat transfer coefficient values for air–water flow with calculated values using Equation (13) for 20 PPI foam.

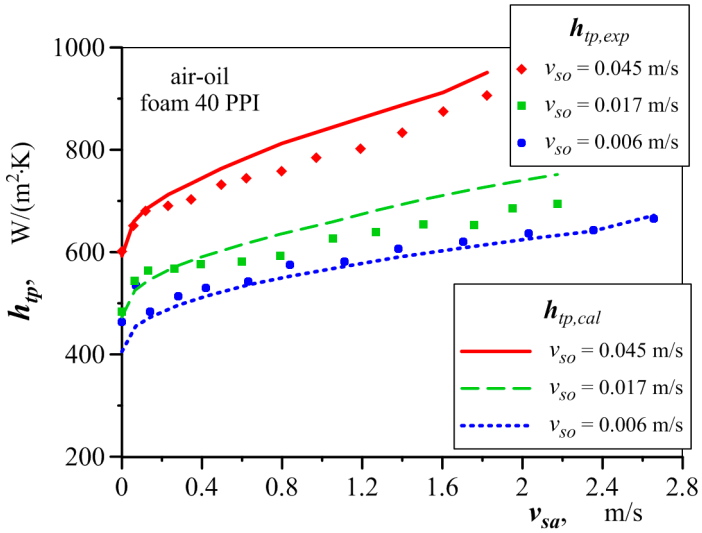

Figure 10. Comparison of measured heat transfer coefficient values in air–oil flow with calculated values using Equation (13) for 40 PPI foam.

The accuracy of the developed computational method was statistically validated. As illustrated in Figure 11, over 90% of the results, representing various flow conditions, fall within a ±20% error margin. This degree of accuracy is deemed highly satisfactory, especially given the challenges of achieving such precision in two-phase flow analysis. The proposed method for calculating the heat transfer coefficient in gas–liquid flow through channels filled with metal foams remains valid even under conditions where one phase diminishes, i.e., as $v_f \rightarrow 0$.

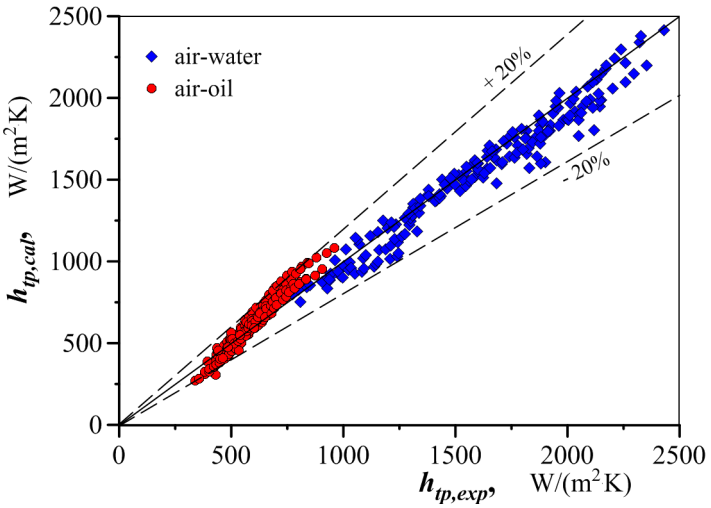

Figure 11. Comparison of measured heat transfer coefficient values in air–oil and air–water flow with calculated values using Equation (13).

5. Conclusions

The experimental studies described in this paper aimed to investigate the influence of flow conditions on heat transfer during the flow of a gas–liquid two-phase mixture through channels filled with metal foams. Particular emphasis was placed on analyzing the impact of flow velocity, the physical properties of both phases, the characteristics of flow structures, as well as the geometric parameters and thermal conductivity of the metal foams. Additionally, it was deemed essential to develop a method for determining the heat transfer coefficient for non-boiling flows in channels packed with metal foams.

The study investigated the flow of two types of gas–liquid mixtures, air–water and air–mineral oil, through pipes filled with three types of open-cell aluminum foams with pore densities of 20, 30, and 40 PPI. The corresponding cell sizes of the foams were 3.45, 2.25, and 2.39 mm, respectively. The porosity of the foams ranged between 92.9% and 94.3%. The measurements were conducted over a range of superficial gas velocities from 0.060 to 2.264 m/s and liquid velocities from 0.006 to 0.063 m/s. The volumetric gas fraction in the two-phase mixture varied between 0.488 and 0.988. A total of 360 heat transfer coefficient values were obtained from the measurements. Based on the analysis of the collected data and a comprehensive review of the relevant literature, the following conclusions have been formulated, which, in the context of the established research objectives, can be divided into three key groups.

The influence of flow conditions—A significant impact of phase velocities, flow turbulence, liquid viscosity, and thermal properties of the fluids was observed.

- In gas–liquid flow through metal foams, the heat transfer coefficient is generally higher compared to single-phase gas or liquid flows.
- The heat transfer coefficient increases with the rise in superficial velocity of each phase. In the air–water flow, this increase is exponential with an exponent less than 1. In the case of air–oil flow, the variation in the heat transfer coefficient (h_{tp}) with increasing air velocity resembles a linear function, as the flow involving oil exhibits a laminar character over a wide range of phase velocity variations.
- The lower turbulence of the air–oil flow results in a heat transfer coefficient that is more than two times smaller compared to the values obtained under the same flow conditions for air–water flow. In the studies, the heat transfer coefficient values were recorded as h_{tp} = 340–1082 W/(m^2·K) for the air–oil flow and h_{tp} = 754–2430 W/(m^2·K) for the air–water flow. Furthermore, oil has a thermal conductivity that is more than four times lower than that of water, which further diminishes the intensity of heat transfer.
- Liquids play a crucial role in heat transfer. The significant mass fraction of liquid in the mixture, even with a considerable volumetric fraction of air, along with the high intensity of heat transfer into the liquid, enables this phase to absorb up to 800 times more heat when compared to equivalent flow rates of gas and liquid. A tenfold increase in the air flow rate results in a maximum enhancement of the heat transfer coefficient by 17%. In contrast, an equivalent increase in the liquid flow rate leads to an approximate rise of 65% in the heat transfer coefficient for oil and about 90% for water.
- The intensity of heat transfer in stratified flow is lower compared to other flow regimes. Under conditions of transition from plug or slug flow to stratified flow, a sudden reduction in the heat transfer coefficient occurs by several percentage points, despite an increase in gas velocity. This phenomenon was observed solely in the case of air–water flow.

The influence of metal foam—Analyses have demonstrated a significant impact of geometric parameters and the thermal conductivity of the foam's structure on the heat transfer process. Although this influence is noticeable, it is generally less pronounced than the effects of hydrodynamic conditions and the physical properties of the fluids.

- Differences in the heat transfer coefficient for flows through the examined metal foams, under identical air–water flow conditions, can reach up to 50%. In contrast, for air–oil flows, these differences do not exceed 20%. This observation highlights the significance of fluid properties in heat transfer during flow through metal foams.
- The highest intensity of heat transfer was recorded for the flow through 20 PPI foams, which exhibit the largest cell size among the utilized foams. The larger cells promote the development of turbulent flow, which compensates for the lower specific surface area of the 20 PPI foam compared to foams with higher pore densities.

- Similar values of the heat transfer coefficient were observed during the flow through the 40 PPI foam, which is characterized by the smallest cells. However, it is noteworthy that the skeleton material of this foam exhibits a thermal conductivity that is 26% higher compared to the 20 PPI and 30 PPI foams.

Prediction of the heat transfer coefficient value

- The methods developed for predicting the heat transfer coefficient in two-component non-boiling flows through empty channels or boiling flows through metal foam-filled channels are not applicable to two-component non-boiling flows through channels filled with metal foams. The accuracy of the results obtained using these methods is insufficient. Among the analyzed methods, the approach by Rezkallah et al. [76] demonstrates the smallest average error of 40%; however, the resulting values of the heat transfer coefficient exhibit an incorrect trend with respect to air velocity.
- The heat transfer coefficient in non-boiling flows through channels filled with metal foams can be derived from the coefficients for single-phase gas and liquid flows, considering phase interactions. This interaction is represented in a newly developed correlation (Equation (21)), which quantifies the enhancement of heat transfer intensity in two-phase flows compared to single-phase flows.
- The value of the heat transfer coefficient in non-boiling flows through channels filled with metal foams can be determined based on the set of Equations (13)–(21) developed in this study. These equations constitute a comprehensive computational model that provides satisfactory accuracy in predicting the value of the heat transfer coefficient; 90% of the results fall within a margin of error not exceeding 20%. This model can be applied to horizontally heated channels filled with metal foams similar to those used in the study, through which flow mixtures of gas and liquids with low viscosity—up to 10 times greater than the viscosity of water—regardless of the type of flow structure. The model is valid for the flow conditions specified in Table 3. The application of the model over a wider range of hydrodynamic conditions requires further validation.

Author Contributions: Conceptualization, R.D.; Methodology, R.D. and M.P.; Validation, R.D. and M.P.; Investigation, R.D.; Writing—original draft, R.D. and M.P.; Writing—review & editing, M.P.; Visualization, R.D. and M.P.; Supervision, R.D. All authors have read and agreed to the published version of the manuscript.

Funding: This research received no external funding.

Data Availability Statement: All material is available upon request to interested researchers.

Conflicts of Interest: The authors declare no conflict of interest.

Glossary

Nomenclature

a_{sf}	metal foam specific surface area, m^2/m^3
A	total heat transfer area (channel and the foam), m^2
A_{ch}	channel area, m^2
A_{sf}	foam area, m^2
c	specific heat, J/(kg·K)
d_c	cell diameter, m
d	channel diameter, m
d_l	diameter of foam skeleton ligament, m
d_p	pore diameter, m
f	Fanning friction factor, -
g	mass flux, kg/(m^2·s)
h	heat transfer coefficient, W/(m^2·K)
h_{cb}	convective boiling heat transfer coefficient, W/(m^2·K)
h_{nb}	nucleate boiling heat transfer coefficient, W/(m^2·K)

k_s	skeleton thermal conductivity coefficient, W/(m·K)
k_{eff}	effective thermal conductivity coefficient, W/(m·K)
K	foam permeability, m^2
L	channel length, m
m	mass flow rate, kg/s
Nu	Nusselt number, -
Pr	Prandtl number, -
R	void fraction, -
Re	Reynolds number, -
r	heat of vaporization, J/kg
S	heat transfer area, m^2
q	heat flux, W/m^2
Q	heat, W
t	temperature, °C
v_s	superficial velocity (related to the cross-sectional area of the empty channel (without filling)), m/s
V	volume flow rate, m^3/s
x	mass fraction of vapor, -
Greek symbols	
$\Delta p/\Delta l$	unit pressure drop, Pa/m
Δt	temperature difference, K
ϕ	porosity of metal foam, -
ε	inlet volume fraction, -
μ	viscosity, Pa·s
ρ	density, kg/m^3
Θ_{dry}	dry angle, ^{o}
ω	pore density, PPI
Subscripts	
g	gas/air
cal	calculated
exp	experimental
in	inlet condition
l	liquid
ol	oil
out	outlet condition
s	solid/foams skeleton
tp	two-phase
b	channel wall
v	vapor
w	water

References

1. Atwater, M.A.; Guevara, L.N.; Darling, K.A.; Tschopp, M.A. Solid State Porous Metal Production: A Review of the Capabilities, Characteristics, and Challenges. *Adv. Eng. Mater.* **2018**, *20*, 1700766. [CrossRef]
2. Patel, N.; Mittal, G.; Agrawal, M.; Pradhan, A.K. Aluminum Foam Production, Properties, and Applications: A Review. *Int. J. Met.* **2024**, *18*, 2181–2198. [CrossRef]
3. Hassan, A.; Alnaser, I.A. A Review of Different Manufacturing Methods of Metallic Foams. *ACS Omega* **2024**, *9*, 6280–6295. [CrossRef]
4. Kumar, K.; Ingole, S.B.; Saeedjassim, A.; Gori, Y.; Kaushik, A.; Kumar, D.; Jain, A. Aluminum-Foam by Powder Metallurgy: A Review. *Mater. Today Proc.* 2023. [CrossRef]
5. du Plessis, A.; Razavi, N.; Benedetti, M.; Murchio, S.; Leary, M.; Watson, M.; Bhate, D.; Berto, F. Properties and Applications of Additively Manufactured Metallic Cellular Materials: A Review. *Prog. Mater. Sci.* **2022**, *125*, 100918. [CrossRef]
6. Ahmed, H.E.; Fadhil, O.T.; Salih, W.A. Heat Transfer and Fluid Flow Characteristics of Tubular Channel Partially Filled with Grooved Metal Foams. *Int. Commun. Heat Mass Transf.* **2019**, *108*, 104336. [CrossRef]

7. Alhusseny, A.N.M.; Nasser, A.G.; Al-zurf, N.M.J. High-Porosity Metal Foams: Potentials, Applications, and Formulations. In *Porosity—Process, Technologies and Applications*; IntechOpen: London, UK, 2018.
8. Jeong, C.H.; Kim, H.R.; Ha, M.Y.; Son, S.W.; Lee, J.S.; Kim, P.Y. Metal Foams: Fundamentals and Applications | Metal Foams: Fundamentals and Applications, Nihad Dukhan (Ed.), University of Detroit Mercy, DEStech Publications, Inc., Lancaster, PA, USA (2013), ISBN:978-1-60595-014-3, $US189.50. *Appl. Therm. Eng.* **2013**, *61*, 1. [CrossRef]
9. Kuruneru, S.T.W.; Vafai, K.; Sauret, E.; Gu, Y.T. Application of Porous Metal Foam Heat Exchangers and the Implications of Particulate Fouling for Energy-Intensive Industries. *Chem. Eng. Sci.* **2020**, *228*, 115968. [CrossRef]
10. Zhou, F.; Lu, T.; Ding, G.; Yang, G. Experimental Research on Flow Mode Transition of Falling Film Flow on Metal Foam Wrapped Tubes. *Exp. Therm. Fluid Sci.* **2020**, *118*, 110154. [CrossRef]
11. Dineshkumar, J.; Jesudas, T.; Elayaraja, R. Characteristics, Applications and Processing of Aluminium Foams—A Review. *Proc. Mater. Today Proc.* **2021**, *42*, 1773–1776. [CrossRef]
12. Zhao, C.Y. Review on Thermal Transport in High Porosity Cellular Metal Foams with Open Cells. *Int. J. Heat Mass Transf.* **2012**, *55*, 3618–3632. [CrossRef]
13. Zaib, F.; Ganesan, P.; Zaharinie, T.; Chen, Z.; Naganthran, K. Heat Transfer Performance of a Compact Heat Exchanger Based on Metal Foam and Thermal Interface Material (TIM). *Int. J. Heat Mass Transf.* **2024**, *231*, 125861. [CrossRef]
14. Muneeshwaran, M.; Yang, C.M.; Cakmak, E.; Nawaz, K. Augmentation of Pool Boiling Heat Transfer on Tube Bundles Using Metal Foam. *Appl. Therm. Eng.* **2024**, *236*, 121812. [CrossRef]
15. Xiong, J.; Sun, J.; Chen, Y.; Nie, Z. Study on the Flow and Heat Transfer Characteristics inside High-Porosity Open-Cell Copper Foams: Experimental and Numerical Explorations. *Int. J. Heat Fluid Flow* **2024**, *109*, 109499. [CrossRef]
16. Huisseune, H.; De Schampheleire, S.; Ameel, B.; De Paepe, M. Comparison of Metal Foam Heat Exchangers to a Finned Heat Exchanger for Low Reynolds Number Applications. *Int. J. Heat Mass Transf.* **2015**, *89*, 1–9. [CrossRef]
17. Abadi, G.B.; Moon, C.; Kim, K.C. Flow Boiling Visualization and Heat Transfer in Metal-Foam-Filled Mini Tubes—Part I: Flow Pattern Map and Experimental Data. *Int. J. Heat Mass Transf.* **2016**, *98*, 857–867. [CrossRef]
18. Hafeez, P. Heat Transfer in Metal Foam Heat Exchangers at High Temperature. Ph.D. Thesis, University of Toronto, Toronto, ON, Canada, 2016.
19. Kouidri, A.; Madani, B. Thermal and Hydrodynamic Performance of Flow Boiling through a Heat Exchanger Filled with Various Metallic Foam Samples. *Chem. Eng. Process. Process Intensif.* **2017**, *121*, 162–169. [CrossRef]
20. Nam, S.; Kim, D.Y.; Kim, Y.; Kim, K.C. Effect of Metal Foam Insert Configurations on Flow Boiling Heat Transfer and Pressure Drop in a Rectangular Channel. *Materials* **2021**, *14*, 4617. [CrossRef]
21. Chen, K.; Guo, L.; Wang, H. A review on thermal application of metal foam. *Sci. China Technol. Sci.* **2020**, *63*, 2469–2490. [CrossRef]
22. Athith, T.S.; Trilok, G.; Jadhav, P.H.; Gnanasekaran, N. Heat Transfer Optimization Using Genetic Algorithm and Artificial Neural Network in a Heat Exchanger with Partially Filled Different High Porosity Metal Foam. *Proc. Mater. Today Proc.* **2022**, *51*, 1642–1648. [CrossRef]
23. Chatzi, P.; Efstathiadis, T.; Skordos, A.A.; Kalfas, A.I. Metal Foam Recuperators on Micro Gas Turbines: Multi-Objective Optimisation of Efficiency, Power and Weight. *Appl. Therm. Eng.* **2024**, *242*, 122410. [CrossRef]
24. Bai, Y.; Pu, Y.; Chang, C.; Zhang, Y.; Kang, X. Investigation of the Unsteady Thermal Storage Performance of Metal Foam Dual-Phase Change Unit Thermal Storage Tanks in Solar Thermal Utilization Systems. *Appl. Therm. Eng.* **2024**, *250*, 123477. [CrossRef]
25. NematpourKeshteli, A.; Iasiello, M.; Langella, G.; Bianco, N. Using Metal Foam and Nanoparticle Additives with Different Fin Shapes for PCM-Based Thermal Storage in Flat Plate Solar Collectors. *Therm. Sci. Eng. Prog.* **2024**, *52*, 102690. [CrossRef]
26. Bianco, N.; Cherella, N.; Fragnito, A.; Iasiello, M.; Mauro, G.M. Multi-Material Topology Optimization of Innovative Microchannel Heat Sinks Equipped with Metal Foams. *Int. J. Heat Mass Transf.* **2024**, *222*, 125201. [CrossRef]
27. Salim, B.; Abdenour, S.; Oualid, C.; Marwani, H.M.; Sami, R.; Aljuraide, N.I.; Althomali, R.H.; Rahman, M.M.; Ali, M.M.; El Bouz, M.A. Three-Dimensional Transient CFD Modeling of Multiple Finned Aluminum Foam Heat Sinks in a Horizontal Channel. *Alex. Eng. J.* **2023**, *78*, 426–437. [CrossRef]
28. Xia, G.; Wang, Y.; Li, R.; Yan, Z.; Li, Q. Experimental Study of Boiling Heat Transfer Characteristics of Metal Foam Porous-Wall Mini-Channels. *Int. J. Refrig.* **2023**, *151*, 278–289. [CrossRef]
29. Ami Ahmadi, H.; Variji, N.; Kaabinejadian, A.; Moghimi, M.; Siavashi, M. Optimal Design and Sensitivity Analysis of Energy Storage for Concentrated Solar Power Plants Using Phase Change Material by Gradient Metal Foams. *J. Energy Storage* **2021**, *35*, 102233. [CrossRef]
30. Wang, Y.; Yu, Y.; Jing, Z.; Wang, C.; Zhou, G.; Zhao, W. Thermal Performance of Lithium-Ion Batteries Applying Forced Air Cooling with an Improved Aluminium Foam Heat Sink Design. *Int. J. Heat Mass Transf.* **2021**, *167*, 120827. [CrossRef]
31. Li, Y.; Gong, L.; Xu, M.; Joshi, Y. A Review of Thermo-Hydraulic Performance of Metal Foam and Its Application as Heat Sinks for Electronics Cooling. *J. Electron. Packag.* **2021**, *143*, 030801. [CrossRef]
32. Shenming, X.; Ran, Y.; Limei, S.; Yupeng, W.; Junlong, X.; Huanxin, C. The Experimental Study of a Novel Metal Foam Heat Pipe Radiator. *Proc. Energy Procedia* **2019**, *158*, 5439–5444. [CrossRef]
33. Welsford, C.A.; Delisle, C.S.; Plant, R.D.; Saghir, M.Z. Effects of Nanofluid Concentration and Channeling on the Thermal Effectiveness of Highly Porous Open-Cell Foam Metals: A Numerical and Experimental Study. *J. Therm. Anal. Calorim.* **2020**, *140*, 1507–1517. [CrossRef]

34. Wan, Z.; Sun, Y.; Yang, C. Design Strategy of Metal Foam Flow Field and Its Application in Proton Exchange Membrane Fuel Cell. In *Transport Perspectives for Porous Medium Applications*; IntechOpen: London, UK, 2024.
35. Chen, Z.; Zuo, W.; Zhou, K.; Li, Q.; Huang, Y.; E, J. Multi-Objective Optimization of Proton Exchange Membrane Fuel Cells by RSM and NSGA-II. *Energy Convers. Manag.* **2023**, *277*, 116691. [CrossRef]
36. Chen, Z.; Zuo, W.; Zhou, K.; Li, Q.; Huang, Y.E.J. Multi-factor impact mechanism on the performance of high temperature proton exchange membrane fuel cell. *Energy* **2023**, *278*, 127982. [CrossRef]
37. Chen, Z.; Zuo, W.; Zhou, K.; Li, Q.; Yi, Z.; Huang, Y. Numerical investigation on the performance enhancement of PEMFC with gradient sinusoidal-wave fins in cathode channel. *Energy* **2024**, *288*, 129894. [CrossRef]
38. Jaisatia Varthani, A.; Shasthri, S.; Baljit, S.; Kausalyah, V. A Systematic Review of Metal Foam and Heat Pipe Enhancement in Latent Heat Thermal Energy Storage System. *J. Energy Storage* **2022**, *56*, 105888. [CrossRef]
39. Zhu, Y.; Hu, H.; Ding, G.; Sun, S.; Jing, Y. Influence of Metal Foam on Heat Transfer Characteristics of Refrigerant-Oil Mixture Flow Boiling inside Circular Tubes. *Proc. Appl. Therm. Eng.* **2013**, *50*, 1246–1256. [CrossRef]
40. Zhu, Y.; Hu, H.; Sun, S.; Ding, G. Flow Boiling of Refrigerant in Horizontal Metal-Foam Filled Tubes: Part 2—A Flow-Pattern Based Prediction Method for Heat Transfer. *Int. J. Heat Mass Transf.* **2015**, *91*, 502–511. [CrossRef]
41. Mancin, S.; Diani, A.; Doretti, L.; Rossetto, L. R134a and R1234ze(E) Liquid and Flow Boiling Heat Transfer in a High Porosity Copper Foam. *Int. J. Heat Mass Transf.* **2014**, *74*, 77–87. [CrossRef]
42. Samir, A.; Hussain, I.Y. Simulation of Natural Convection Boiling Heat Transfer for Refrigerant R-134a Flow in a Metal Foam Filled Vertical Tube. *Case Stud. Therm. Eng.* **2019**, *13*, 100390. [CrossRef]
43. Bamorovat Abadi, G.; Moon, C.; Kim, K.C. Flow Boiling Visualization and Heat Transfer in Metal-Foam-Filled Mini Tubes—Part II: Developing Predictive Methods for Heat Transfer Coefficient and Pressure Drop. *Int. J. Heat Mass Transf.* **2016**, *98*, 868–878. [CrossRef]
44. Azizifar, S.; Ameri, M.; Behroyan, I. Subcooled Flow Boiling of Water in a Metal-Foam Tube: An Experimental Study. *Int. Commun. Heat Mass Transf.* **2020**, *118*, 104897. [CrossRef]
45. Weise, S.; Wetzel, T.; Dietrich, B. Influence of Porous Inserts on Flow Boiling Heat Transfer in Horizontal Tubes. *Int. J. Heat Mass Transf.* **2021**, *171*, 121087. [CrossRef]
46. Li, H.W.; Zhang, C.Z.; Yang, D.; Sun, B.; Hong, W.P. Experimental Investigation on Flow Boiling Heat Transfer Characteristics of R141b Refrigerant in Parallel Small Channels Filled with Metal Foam. *Int. J. Heat Mass Transf.* **2019**, *133*, 21–35. [CrossRef]
47. Bamorovat Abadi, G.; Kim, K.C. Enhancement of Phase-Change Evaporators with Zeotropic Refrigerant Mixture Using Metal Foams. *Int. J. Heat Mass Transf.* **2017**, *106*, 908–919. [CrossRef]
48. Nosrati, A.; Akhavan-Behabadi, M.A.; Sajadi, B.; Razi, P.; Mohammadi, R. Experimental Study on the Effects of Using Metal Foam on R-134a Flow Boiling in Annular Tubes. *Int. J. Therm. Sci.* **2022**, *177*, 107546. [CrossRef]
49. Haertlé, S. Flow Boiling of CO_2 in Porous Structures. Ph.D. Thesis, Karlsruher Instituts für Technologie, Karlsruhe, Germany, 2022. [CrossRef]
50. Liaw, K.L.; Kurnia, J.C.; Sallih, N.; Mustapha, M.; Sasmito, A.P. Heat Transfer Analysis of Subcooled Flow Boiling in Copper Foam Helical Coiled Heat Exchanger—A Pore-Scale Numerical Study. *Int. Commun. Heat Mass Transf.* **2024**, *155*, 107514. [CrossRef]
51. Zhu, Y.; Hu, H.; Sun, S.; Ding, G. Heat Transfer Measurements and Correlation of Refrigerant Flow Boiling in Tube Filled with Copper Foam. *Int. J. Refrig.* **2014**, *38*, 215–226. [CrossRef]
52. Zhu, Y.; Hu, H.; Sun, S.; Ding, G. Flow Boiling of Refrigerant in Horizontal Metal-Foam Filled Tubes: Part 1-Two-Phase Flow Pattern Visualization. *Int. J. Heat Mass Transf.* **2015**, *91*, 446–453. [CrossRef]
53. Gao, W.; Xu, X.; Liang, X. Flow Boiling of R134a in an Open-Cell Metal Foam Mini-Channel Evaporator. *Int. J. Heat Mass Transf.* **2018**, *126*, 103–115. [CrossRef]
54. Hu, H.; Lai, Z.; Zhao, Y. Heat Transfer and Pressure Drop of Refrigerant Flow Boiling in Metal Foam Filled Tubes with Different Wettability. *Int. J. Heat Mass Transf.* **2021**, *177*, 121542. [CrossRef]
55. Hu, H.; Zhao, Y.; Sheng, J.; Li, Y. Influence of Surface Wettability on Heat Transfer and Pressure Drop Characteristics of R1234ze(E) Flow Boiling in Metal Foam Filled Tubes. *Int. J. Refrig.* **2023**, *146*, 366–374. [CrossRef]
56. Wang, X.W.; Ho, J.Y.; Leong, K.C.; Wong, T.N. Condensation Heat Transfer and Pressure Drop Characteristics of R-134a in Horizontal Smooth Tubes and Enhanced Tubes Fabricated by Selective Laser Melting. *Int. J. Heat Mass Transf.* **2018**, *126*, 949–962. [CrossRef]
57. Shi, J.; Zheng, G.; Chen, Z. Experimental Investigation on Flow Condensation in Horizontal Tubes Filled with Annular Metal Foam. *Int. J. Heat Mass Transf.* **2018**, *116*, 920–930. [CrossRef]
58. Shi, J.; Zheng, G.; Chen, Z.; Dang, C. Experimental Study of Flow Condensation Heat Transfer in Tubes Partially Filled with Hydrophobic Annular Metal Foam. *Int. J. Heat Mass Transf.* **2019**, *136*, 1265–1272. [CrossRef]
59. Tourvieille, J.N.; Philippe, R.; de Bellefon, C. Milli-channel with metal foams under an applied gas-liquid periodic flow: Flow patterns, residence time distribution and pulsing properties. *Chem. Eng. Sci.* **2015**, *126*, 406426. [CrossRef]
60. Lali, F. A hydrodynamic study of cylindrical metal foam packings: Residence time distribution and two phase pressure drop. *Chem. Eng. Proc.* **2017**, *115*, 1–10. [CrossRef]
61. Hessel, V.; Angeli, P.; Gavriilidis, A.; Löwe, H. Gas–Liquid and Gas–Liquid–Solid Microstructured Reactors: Contacting Principles and Applications. *Ind. Eng. Chem. Res.* **2005**, *44*, 9750–9769. [CrossRef]

62. Walchi, S. Two-Phase Flow Characterictics in Gas-Liquid Microreactors. Ph.D. Thesis, Swiss Federal Institute of Technology Zurich, Zürich, Switzerland, 2005.
63. Losey, M.W.; Jackman, R.J.; Firebaugh, S.L.; Schmidt, M.A.; Jensen, K.F. Design and fabrication of microfluidic devices for multiphase mixing and reaction. *J. Microelectromech. Syst.* **2002**, *11*, 709–717. [CrossRef]
64. Xue, H.; Qi, T.; Su, W.; Wu, K.J.; Su, A. Heterogeneous Continuous Flow Hydrogenation of Hexafluoroacetone Trihydrate and Its Kinetic Modeling. *Ind. Eng. Chem. Res.* **2023**, *62*, 6121–6129. [CrossRef]
65. Dyga, R.; Brol, S. Pressure Drops in Two-Phase Gas–Liquid Flow through Channels Filled with Open-Cell Metal Foams. *Energies* **2021**, *14*, 2419. [CrossRef]
66. JCGM Evaluation of Measurement Data—Guide to the Expression of Uncertainty in Measurement; Joint Committee for Guides in Metrology 2008, JCGM 100:2008. p. 120. Available online: https://www.bipm.org/documents/20126/2071204/JCGM_100_2008_E.pdf (accessed on 17 October 2024).
67. Brol, S.; Dyga, R. Self-Affinity Approach for the Determination of Flow Regime in Pipelines. *Meas. J. Int. Meas. Confed.* **2021**, *168*, 108452. [CrossRef]
68. Dyga, R.; Płaczek, M. Influence of Hydrodynamic Conditions on the Type and Area of Occurrence of Gas-Liquid Flow Patterns in the Flow through Open-Cell Foams. *Materials* **2020**, *13*, 3254. [CrossRef]
69. Płaczek, M.; Dyga, R.; Witczak, S. Experimental Investigation of Void Fraction in Horizontal Air-Water Flow through FeCrAlY Foam. *Proc. Procedia Eng.* **2012**, *42*, 690–703. [CrossRef]
70. Dyga, R.; Płaczek, M. Selected Problems of Gas-Liquid Flow through the Channels Filled with Metal Foams. *Proc. E3S Web Conf.* **2017**, *19*, 03001. [CrossRef]
71. Płaczek, M.; Dyga, R. Void Fraction Prediction Method in Gas–Liquid Flow through Channel Packed with Open-Cell Metal Foams. *Energies* **2021**, *14*, 2645. [CrossRef]
72. Ghajar Afshin, J. Two-Phase Heat Transfer in Gas-Liquid Non-Boiling Pipe Flows. In Proceedings of the 3rd International Conference on Heat Transfer, Fluid Mechanics and Thermodynamics HEFAT 2004, Cape Town, South Africa, 21 June 2004; p. K2.
73. Khoze, A.N.; Dunaev, S.V.; Sparin, V.A. Heat and Mass Transfer in Rising Two-Phase Flows in Rectangular Channels. *Heat Transf. Sov. Res.* **1976**, *8*, 87–90.
74. Kim, D.; Ghajar, A.J. Heat Transfer Measurements and Correlations for Air-Water Flow of Different Flow Patterns in a Horizontal Pipe. *Exp. Therm. Fluid Sci.* **2002**, *25*, 659–676. [CrossRef]
75. Nada, S.A. Experimental Investigation and Empirical Correlations of Heat Transfer in Different Regimes of Air-Water Two-Phase Flow in a Horizontal Tube. *J. Therm. Sci. Eng. Appl.* **2017**, *9*, 021004. [CrossRef]
76. Rezkallah, K.S.; Sims, G.E. An Examination of Correlations of Mean Heat Transfer Coefficients in Two-Phase and Two-Component Flow in Vertical Tubes. In Proceedings of the National Heat Transfer Conference and Exhibition, Pittsburgh, PA, USA, 9–12 August 1987; American Institute of Chemical Engineers: New York, NY, USA, 1987; pp. 109–114.
77. Samir, A.A.; Hussain, I.Y. Experimental investigation of convective boiling heat transfer for r-134a flow in metal foam filled vertical tube. *J. Mech. Contin. Math. Sci.* **2019**, *14*, 168–189. [CrossRef]
78. Dyga, R.; Troniewski, L. Convective Heat Transfer for Fluids Passing through Aluminum Foams. *Arch. Thermodyn.* **2015**, *36*, 139–156. [CrossRef]
79. Noh, J.S.; Lee, K.B.; Lee, C.G. Pressure Loss and Forced Convective Heat Transfer in an Annulus Filled with Aluminum Foam. *Int. Commun. Heat Mass Transf.* **2006**, *33*, 434–444. [CrossRef]

Disclaimer/Publisher's Note: The statements, opinions and data contained in all publications are solely those of the individual author(s) and contributor(s) and not of MDPI and/or the editor(s). MDPI and/or the editor(s) disclaim responsibility for any injury to people or property resulting from any ideas, methods, instructions or products referred to in the content.